Journal Name

ARTICLE

Ammonium chloride-metal hydride based reaction cycle for vehicular applications†

Received 00th January 20xx,
Accepted 00th January 20xx

DOI: 10.1039/x0xx00000x

www.rsc.org/

Helen G. Stewart,‡[a] Terry D. Humphries,‡[a]* Drew A. Sheppard,[a] Mariana S. Tortoza,[a] M. Veronica Sofianos,[a] Shaomin Liu,[b] and Craig E. Buckley[a]

Hydrogen and ammonia have attracted attention as potential energy vectors due to their abundance and minimal environmental impact when used as a fuel source. To be a commercially viable alternative to fossil fuels, gaseous fuel sources must adhere to a wide range of standards specifying hydrogen delivery temperature, gravimetric capacity and cost. In this article, an ammonium chloride-metal hydride reaction cycle that enables the solid thermal decomposition products to be recycled using industrial processes is proposed. A range of metal hydrides and metal amides were reacted with ammonium chloride to determine the reaction pathways, products and overall feasibility of the cycle. The NH_4Cl-*M*H (*M*H = metal hydride) and NH_4Cl-*M*NH_2 (*M*NH_2 = metal amide) mixtures were heated to temperatures of up to 500 °C. The resulting products were experimentally characterised using temperature program desorption residual gas analysis, simultaneous differential scanning calorimetry and thermogravimetric analysis and *in situ* powder X-ray diffraction. Similar analysis was undertaken to determine the effect of catalyst addition to the starting materials. A maximum yield of 41 wt% of hydrogen and ammonia gas mixtures were released from the NH_4Cl-*M*H materials. This exceptional gravimetric capacity allows for volumetric gas densities (363 – 657 kg/m^3) that are much higher than pure NH_3, H_2 or metal hydride materials. Overall, the reaction cycle potentially allows carbon-neutral regeneration of the starting materials, making it a sustainable energy option.

Introduction

With world energy consumption projected to exceed 18,000 TWh by 2035,[1] it has never been more important to invest in the development of sustainable energy technologies to meet this demand. Hydrogen is an attractive potential energy vector. It is universally abundant on earth, and its combustion has minimal environmental impact as it does not produce any carbon dioxide or nitrous oxides. Storing hydrogen in a high volumetric density format that flexibly links its production and use as an energy source is a critical part of developing a hydrogen economy.[2-4]

Hydrogen is traditionally stored in cylinders as a liquid at cryogenic temperatures or as a gas at high pressure.[5] Storage of hydrogen as a high-pressure gas is preferable in industrial facilities and laboratories, where weight and volume capacities are not limiting factors. Storage of hydrogen as a liquid is also not suitable for energy applications as liquefaction can lead to a loss of up to 40% of hydrogen's energy content, while boil-off and safety concerns (through high-pressure build up upon cooling failure) are also factors to consider.[6] Overcoming these barriers and developing a system that can store hydrogen efficiently would provide a long term solution to meeting global energy demands in a sustainable manner.

Metal hydrides are of special interest to the hydrogen storage community. They have the capacity to be developed from inexpensive or abundant materials such as sodium, magnesium, calcium and titanium and form a variety of hydrogen containing species including ionic hydrides, complex hydrides and interstitial hydrides.[7-11] The thermal energy density of metal hydrides is up to thirty times more than molten salts, currently used to store solar energy.[3, 12, 13] They also have the potential to reversibly absorb large amounts of hydrogen which makes them ideal for fuel cell applications.

When in the form of metal hydrides, light metals such as lithium, sodium, magnesium and aluminium are appealing hydrogen storage candidates due to their low atomic weight and high gravimetric hydrogen content.[3, 4, 7-9, 11, 13] The higher the hydrogen-metal ratio and the lighter the metal elements incorporated into these compounds, the higher the hydrogen capacity of the material. Increasing the hydrogen capacity of a material is in effect, increasing its gravimetric energy density. Complex hydrides containing these lightweight metals such as borohydrides, transition metal hydrides, amides, imides and alanates are under investigation for use in hydrogen storage applications due to their potential high hydrogen weight capacities.[2-4, 8, 9]

Ammonia has also been receiving heightened attention as a potential medium of indirect hydrogen storage and as an independent fuel source.[14-16] Ammonia releases 316.80 kJ/mol

[a] *Department of Physics and Astronomy, Fuels and Energy Technology Institute, Curtin University, GPO Box U1987, Perth, WA 6845, Australia.*
[b] *Department of Chemical Engineering, Curtin University, GPO Box U1987, Perth, WA, 6845, Australia.*
* E-mail: terry_humphries81@hotmail.com
†Electronic Supplementary Information (ESI) available: Phase identification of *in situ* XRD data. See DOI: 10.1039/x0xx00000x
‡ These authors contributed equally to this study.

of energy during combustion.[17] This high energy release inspired Green to propose it as an energy vector by Green in 1982.[18] Ammonia's combustion reaction simply releases nitrogen and water (eq. 1), both naturally present in the earth's atmosphere, although a small amount of NO_x may be produced as a by-product.[19] Providing the nitrogen and hydrogen used to synthesise the ammonia are derived from clean and renewable sources, this reaction does not result in the release of hazardous air pollutants such as CO_2, SO_2 and soot.[20] Generally NH_3 has a narrow flammability limit of 15.5% to 27% volume in air,[20] which leads to a low combustion rate. However, recent studies have shown that the presence of hydrogen during ammonia combustion can lower combustion temperatures and increase the burning velocity of ammonia flames. In addition, ammonia-fed solid oxide fuel cells (SOFC) have been developed that can directly utilise ammonia without the requirement for cracking.[21]

$$4NH_{3(g)} + 3O_{2(g)} \rightarrow 2N_{2(g)} + 6H_2O\ (316.8\ kJ/mol{\cdot}NH_3) \quad (1)$$

The Haber-Bosch process[22] has made ammonia readily available at a cost ranging from US$385 to $770 per tonne.[23] In fact, global ammonia production is projected to exceed 150 mega tonnes per annum by the end of the decade.[24] Infrastructure for large-scale ammonia transportation also exists in the form of trucks, tank carriage, barge, ships and pipelines.[25] Therefore, an ammonia based fuel cycle could be expanded to an industrial scale without the need for any new infrastructure. Many factors have prevented the utilisation of ammonia as a large scale commercial fuel source as it is acutely toxic if inhaled, and highly harmful if released into marine environments.[26] The risk associated with ammonia's toxicity can be mitigated by storing it as a solid in the form of metal amines, ammonium chlorides, ammonium carbonates or urea, although infrastructure to retrieve the ammonia from the solid (such as thermal treatment) still needs further development.[27]

In recent studies, ammonium complexes of metal hydrides or metal ammine complexes and metal amines have been under scrutiny as a means of high-density ammonia and hydrogen storage.[14, 16, 28-31] Upon thermal treatment, these complexes produce either NH_3 and/or H_2. Rather than using ammonia directly as a fuel source, David *et al*. have reported a promising method of extracting hydrogen from ammonia or "ammonia cracking".[14] By passing ammonia through a sodium amide catalyst powder they achieved a 99.2% ammonia decomposition efficiency at a temperature of 530 °C. Another technology for an ammonia cracking fuel cell using a zirconium based catalyst has also been patented.[32]

More recently, high purity H_2 (99.99 %) has been produced using a two-step process with initial decomposition using 1 wt % Ru on Al_2O_3 catalyst, followed by purification using Pd-coated tubular vanadium membranes.[33] The catalyst and membrane are operated at temperatures of 450 and 340 °C, respectively. Other reported hydrogen separation membrane systems include Pd, Pd-Ag, vanadium alloys and Nb.[34] Additionally, adsorption of ammonia into zeolites has been shown to be an efficient method to purify H_2 produced from ammonia.[34]

Li and Hurley investigated the effect of the presence of palladium (II) and palladium (IV) chlorides and ammonium chloride on the reaction between ammonia and magnesium hydride.[35] Their results showed that the addition of palladium (II) chloride and ammonium chloride increased the concentration of hydrogen in the released ammonia by up to 20 % compared to a non-doped system. This article, along with a study on the effect of La^{3+} on the dehydrogenation of $LiAlH_4$-NH_4Cl,[36] is one of the few articles in current literature that examines ammonium chloride in a metal hydride system.

For the ammonia cycle to be feasible and especially allow ammonia based materials to be used in vehicular or stationary applications, cracking of ammonia must be achieved at a temperature lower than the current limit of 450 °C in order to reduce energy costs.[37] In fact, for vehicular applications, a conversion temperature of ~100 °C would be ideal, with high density storage of ammonia/hydrogen a necessity. In addition, the cycle must use cost-effective materials that can be reprocessed.

In this study, the reactions of ammonium chloride with sodium, magnesium, lithium and calcium hydrides and sodium and lithium amides have been experimentally characterised to determine the temperature at which gas release occurs. An evolved gas composition of N_2 and H_2 would be ideal for technical applications as this would allow technological applications using a PEM fuel cell. To promote the formation of H_2 rather than NH_3, addition of $PdCl_2$ as a catalyst has been explored. A number of complementary analysis techniques have been employed to determine the reaction pathway and products including temperature program desorption residual gas analysis, simultaneous differential scanning calorimetry and thermogravimetric analysis and *in situ* powder X-ray diffraction. In addition, a cost-effective cycle has been proposed, demonstrating the recyclability of the reaction products.

Experimental

All handling of chemicals was undertaken in an argon-atmosphere Mbraun Unilab glovebox to minimise oxygen (O_2 < 1 ppm) and water (H_2O < 1 ppm) contamination. NH_4Cl (>99.5 %), NaH (>95 %), LiH (−30 mesh, >95.5 %), MgH_2 (hydrogen storage grade), $LiNH_2$ (>99.5 %) and $PdCl_2$ (>99.9 %), all purchased from Sigma Aldrich and $NaNH_2$ (>95 %, Fluka) were used as supplied with no further purification. CaH_2 powder was prepared by the hydrogenation of Ca powder (99%, granular, Sigma Aldrich) under a H_2 pressure of 30 bar and a temperature of 400 °C for 18 h.

The ammonium chloride and metal hydride (*M*H)/metal amide (MNH_2) powders were mixed by ball milling at 450 rpm in a PQ-NO4 Planetary Ball Mill employing tempered steel vials and balls in an Ar atmosphere. A ball-to-powder mass ratio of 15:1 was employed, in 15 cycles of two minutes milling and a two-minute pause, giving a total milling time of 30 minutes. The stoichiometry of the mixed samples are presented in Table 1. The sample catalysed with $PdCl_2$ was prepared by combining the previously BM NH_4Cl + NaH powder with either 1 or 10 mol%

$PdCl_2$ using an agate mortar and pestle for 2 to 3 minutes under an argon atmosphere.

Table 1. Summary of sample compositions and measured decomposition temperatures, mass loss during thermal treatment and reaction products along with calculated costs. The costs are calculated from the cost of the raw materials and the energy produced from the combustion of the relative molar equivalents of NH_3 and H_2 produced during reaction.

Sample	Reaction Onset Temperature (°C) (RGA)	Total Theoretical/ Experimental (TGA) Gravimetric capacity (wt%)	Solid Reaction Products	Gaseous Reaction Products	Theoretical/ Experimental volumetric gas density (kg gas/m^3)	Cost (US$/kWh)[38]	Theoretical enthalpy of combustion (kJ/kg reactant)
NH_4Cl + NaH	90	24.6/ 24.8	NaCl	$H_2 + NH_3$	360/363	0.6	7209
$NH_4Cl + NaNH_2$	94	36.8/ 34.0	NaCl	$2NH_3$	558/496	1.4	6849
$2NH_4Cl + MgH_2$	125	28.6/ 40.4	$MgCl_2$	$2H_2 + 2NH_3$	430/607	0.3	8381
NH_4Cl + LiH	115	31.0 / 37.6	LiCl	$H_2 + NH_3$	364/442	5.2	9092
$NH_4Cl + LiNH_2$	72	44.5 / 38.3	LiCl	$2NH_3$	640/519	15.7	8287
$2NH_4Cl + CaH_2$	120	25.5 / 41.4	$CaCl_2$	$2H_2 + 2NH_3$	406/657	0.5	7494
NH_4Cl + NaH + $PdCl_2$ (1 mol%)	60	24.3/ 28.8	NaCl + Pd	$H_2 + NH_3$	---	---	---

X-Ray diffraction (XRD) was performed using the Bruker AXS D8 Advance Discover XRD System (λ = 1.5406 Å) set at 40 kV and 40 mA. The data was collected with a proportional counter, using a step scan from 2° to 80° 2Θ with 0.03 degree steps for 0.6 s/step. XRD sample holders covered with a poly(methylmethacrylate) (PMMA) airtight dome were used to prevent oxygen/moisture contamination during data collection. The PMMA airtight bubble results in a broad hump in XRD patterns centred at ~20° 2Θ. *In situ* synchrotron powder X-ray diffraction (SR-XRD) was performed at the Australian Synchrotron in Melbourne, Australia.[39] Powdered samples were loaded in a quartz capillary (outer diameter 0.7 mm, wall thickness 0.01 mm) that were then, using graphite ferrules, mounted in 1/16" tube fittings in a glove box filled with purified argon (< 1 ppm O_2 and H_2O). The sample holder was then connected to a H_2 gas filling/vacuum manifold and the capillary heated with a hot air blower with a heating rate of 5 °C/min *in vacuo*. The temperature of the hot-air blower was calibrated against the known thermal expansion coefficients for NaCl and Ag.[40, 41] One-dimensional SR-XRD patterns (monochromatic X-rays with λ = 1.0003896(1) Å) were collected using a Mythen, microstrip detector with an exposure time of 54 s per pattern. The capillary was rotated 120° during exposure to improve the powder averaging. The crystalline phases were identified by reference to the ICDD PDF database. Diffraction patterns were quantitatively analysed with the Rietveld method using the TOPAS software (Bruker-AXS).

TPD-MS (Temperature Programmed Desorption-Mass Spectrometry) was performed on a quadrupole mass spectrometer residual gas analyser (Stanford Research Systems RGA 300). For each measurement, approximately 0.5 mg of sample was outgassed at below 4×10^{-7} mbar over a minimum of 3 hours. While still under vacuum, the samples were heated up to 480 °C at a heating rate of 2 °C/min. Interpretation of the MS data was carried out using RGA Version 3.218.004 (SRS) using *m/e* = 2 for H_2 and 17 for NH_3. Simultaneous Differential Scanning Calorimetry - Thermal Gravimetric Analysis (DSC-TGA) was performed on a Mettler Toledo DSC 3+ using sample masses of ~10 mg at a heating rate of 5 °C/min under an argon flow of 20 mL/min. The temperature accuracy of this instrument is ± 0.2 °C, while the balance has an accuracy of ± 20 µg.

Results and Discussion

Thermal analysis and decomposition pathway

The NH_4Cl and metal hydride mixtures were ball-milled for 30 mins to maximise homogeneity but also minimise any potential reaction that could occur due to the heat generated during the milling process. Any reaction would result in capacity loss of gases evolved during thermal analysis. Table 1 summarises each of the mixtures employed in this study along with primary results of thermal experiments including DSC-TGA-RGA and also theoretical thermodynamic calculations.

Thermal decomposition of pure NH_4Cl

The decomposition of commercial ammonium chloride was measured by *in situ* SR-XRD and DSC-TGA (Figs. 1 and S1†) to allow direct comparison against the decomposition pathway of the measured NH_4Cl-*M*H and NH_4Cl-*M*NH_2 powder mixtures. The DSC data shows two endothermic events with peak maxima at 190 °C (corresponding to the phase II (LT-NH_4Cl) and phase I (HT-NH_4Cl) solid-solid phase transition), and 310 °C (corresponding to the decomposition of NH_4Cl), which was in agreement with literature values.[42, 43] The TGA shows a distinct sublimation onset at ~208 °C, ending at ~330 °C, with a total

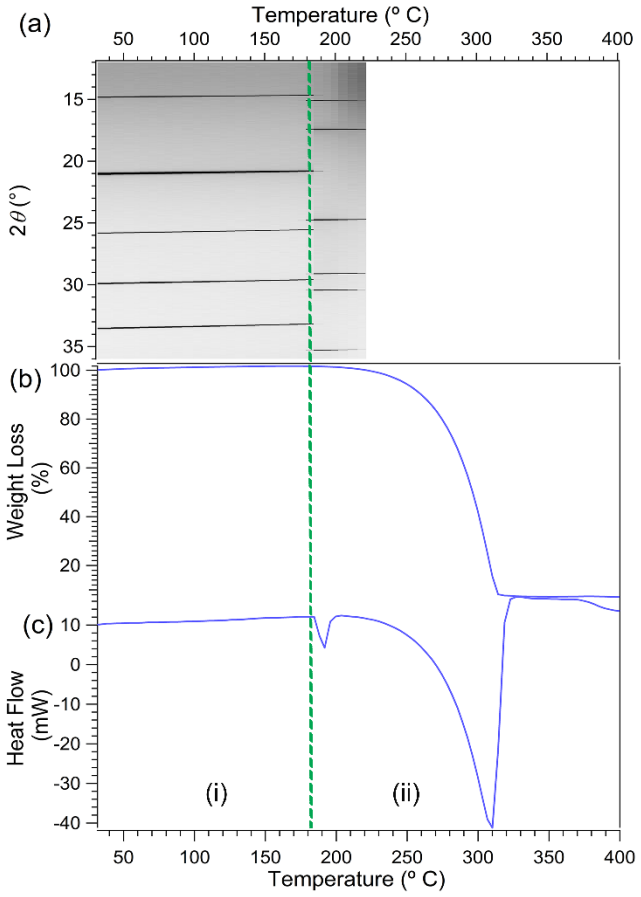

Fig. 1. (a) *In situ* SR-XRD data, (b) TGA and (c) DSC data for NH_4Cl. Region (i): contains LT-NH_4Cl phase. Region (ii) contains HT-NH_4Cl phase. For complete phase identification of XRD data see Fig. S1. $\Delta T/t$ = 5 °C/min. λ = 1.0003896(1) Å. Endothermic heat flow in the down direction for DSC data.

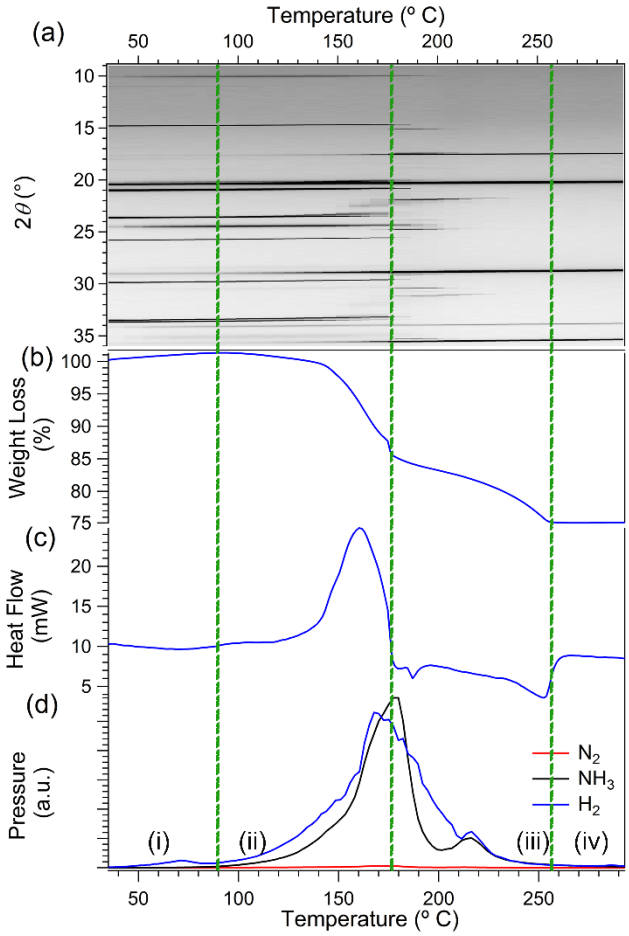

Fig. 2. (a) *In situ* SR-XRD data, (b) TGA, (c) DSC and (d) RGA data for NH_4Cl + NaH. Region (i): contains NaH, LT-NH_4Cl, NaOH and NaCl phases. Region (ii): contains NaH, LT-NH_4Cl, NaOH and NaCl phases. Region (iii) contains NaCl, NaOH and HT-NH_4Cl phases. Region (iv) contains NaCl. For complete phase identification of XRD data see Fig. S2. $\Delta T/t$ = 5 °C/min. λ = 1.0003896(1) Å. Endothermic heat flow in the down direction for DSC data.

mass loss of 94 wt%, allowing for the purity of the starting material.

The *in situ* SR-XRD data corroborates the thermal analysis results. Phase analysis of the material shows that the material at room temperature has Bragg peaks corresponding to LT-NH_4Cl only (space group (SG) $Pm\bar{3}m$). At ~190 °C there is a phase change corresponding to the solid-solid phase transition from the LT-NH_4Cl to HT-NH_4Cl (SG $Fm\bar{3}m$) followed by the subsequent start of decomposition at ~200 °C.

Thermal decomposition of NH_4Cl + NaH

Quantitative analysis of the SR-XRD data of the starting material at room temperature (RT) indicates that the BM material consists of NH_4Cl (66.3(2) wt%), NaH (29.3(2) wt%), NaOH (2.2(2) wt%) and NaCl (2.1(1) wt%) (Figs. 2a and S2†). The small quantity of NaCl observed at RT can only be distinguished by the [022] reflection at 2θ = 29.0° due to the [002] (2θ = 20.4°) reflection being overlapped by the [111] peak of NaH. At ~100 °C the [022] reflection for NaCl clearly starts to increase in intensity corresponding to the onset of decomposition with a corresponding initial gas detection at ~90 °C for the RGA and TGA (Fig. 2b, d, Region (i) and Fig. S2). The first decomposition event is exothermic having a maximum heat flow at 161 °C and ending at ~180 °C (Fig. 2c). Coincidentally, NaH is no longer observed by SR-XRD after ~185 °C, while any remaining LT-NH_4Cl transitions to the HT phase, which is denoted by an endothermic peak by DSC (peak max = 187 °C). In addition, a splitting of the NaH Bragg peaks is observed to occur above 100 °C which is associated with the dissolution of NaOH impurities into the NaH lattice.[11] From TGA, the mass loss in the first decomposition step was measured as 16.8 %, while quantitative Rietveld refinement determined that 85 wt% of NH_4Cl has been consumed along with 100 % NaH, giving a weight loss of 16% consisting of $0.85NH_3$ and $0.925H_2$.

The remaining NH_4Cl decomposes in an endothermic process, with a maximum rate of H_2 and NH_3 release at ~215 °C, leaving NaCl as the only crystalline product. For the remaining HT-NH_4Cl to not decompose into HCl and NH_3, a Na source, other than NaCl, must be present in order to form NaCl, H_2 and NH_3. Crystalline NaOH is still present up to ~200 °C allowing for a Na source. Beyond this temperature, it is likely that an amorphous NaOH species may exist. This is corroborated by the fact that only H_2 and NH_3 were observed by RGA above 200°C. Overall, a

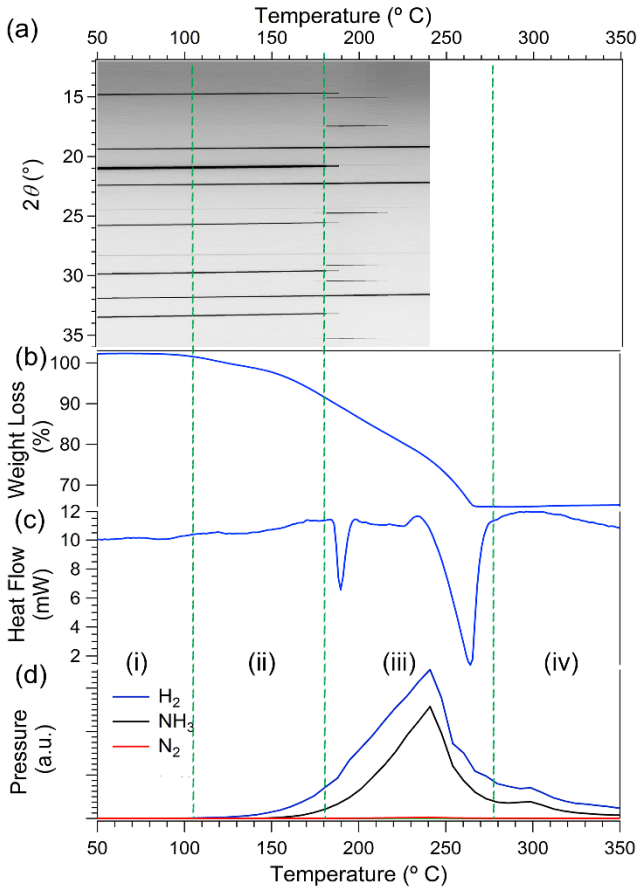

Fig. 3. (a) *In situ* SR-XRD data, (b) TGA, (c) DSC and (d) RGA data for NH_4Cl + LiH. Region (i and ii): contains LiH, LT-NH_4Cl and LiCl phases. Region (iii) contains LiCl and HT-NH_4Cl phases. Region (iv) contains LiCl. For complete phase identification of XRD data see Fig. S4†. $\Delta T/t$ = 5 °C/min. λ = 1.0003896(1) Å. Endothermic heat flow in the down direction for DSC data.

total mass loss of 24.8 wt% was measured before 260 °C, which is close to the expected mass loss of 24.6 wt%.

Thermal decomposition of NH_4Cl + LiH

Initial laboratory based XRD of the NH_4Cl + LiH starting materialat *RT* directly after BM indicates that the material consisted of LT-NH_4Cl (89(2) wt%), LiH (10(2) wt%) and LiCl (1.0(2) wt%) (Fig. S3†), indicating that negligible decomposition occurred during the process. After eight months of storage at *RT* under an Ar atmosphere SR-XRD was conducted. At this point some decomposition had occurred with a composition of NH_4Cl (78.2(5) wt%), LiH (8.4(5) wt%) and LiCl (13.4(1) wt%) being determined (Figs. 3a, S3 and S4†). This suggests that the mixture of these two materials is only metastable. According to the RGA data (Fig. 3d), onset of H_2 desorption occurs at 115 °C, while NH_3 was not detected until 145 °C. The SR-XRD data shows that at ~135 °C the LiCl phase ([111] Bragg peak at ~2Θ = 19.2°), by observation of the data, starts to increase in intensity while at 182 °C the LT-NH_4Cl phase disappears ([011] Bragg peak at ~2Θ = 20.8°) with some undergoing a phase transformation to HT-NH_4Cl. At ~200 °C quantitative Rietveld refinement determines that the sample consists of HT-NH_4Cl (38.9(4) wt%), LiCl (58.1(5) wt%) and LiH (3.0(6) wt%). The initial quantity of LiH may be diminished compared to the theoretical value due to the reduced X-ray scattering of the light Li and H atoms compared to N and Cl. As a result, the peaks for LiH are barely visible in the initial diffraction pattern thus quantification by XRD may not be totally dependable throughout.

The remaining HT-NH_4Cl decomposes in an endothermic process having a maximum heat flow at 264 °C (Fig. 3c) and a peak desorption rate measured by RGA for both H_2 and NH_3 at 241 °C. The final crystalline product is LiCl although 2.5(6) wt% LiH was also observed upon completion of the XRD experiment. Overall a total mass loss of 35.5 wt% was measured below 268 °C by TGA (Fig. 3b), which is close to the theoretical mass loss of 31.0 wt%. There are subtle variations of an otherwise linear wieght change in this region which are most easily observed in the derivative of the TGA pattern (Fig. S5†). As LiH is still observable at the end of the *in situ* SR-XRD experiment, the exaggerated mass loss of an additional 4.5 % may be attributed to the direct decomposition of NH_4Cl into NH_3 and HCl. Although HCl was not detected by RGA, the gas release profile of NH_3 and H_2 appear to be similar and it may be assumed that the HCl may react with the stainless steel tubing producing H_2 at the same rate as NH_3 is detected.

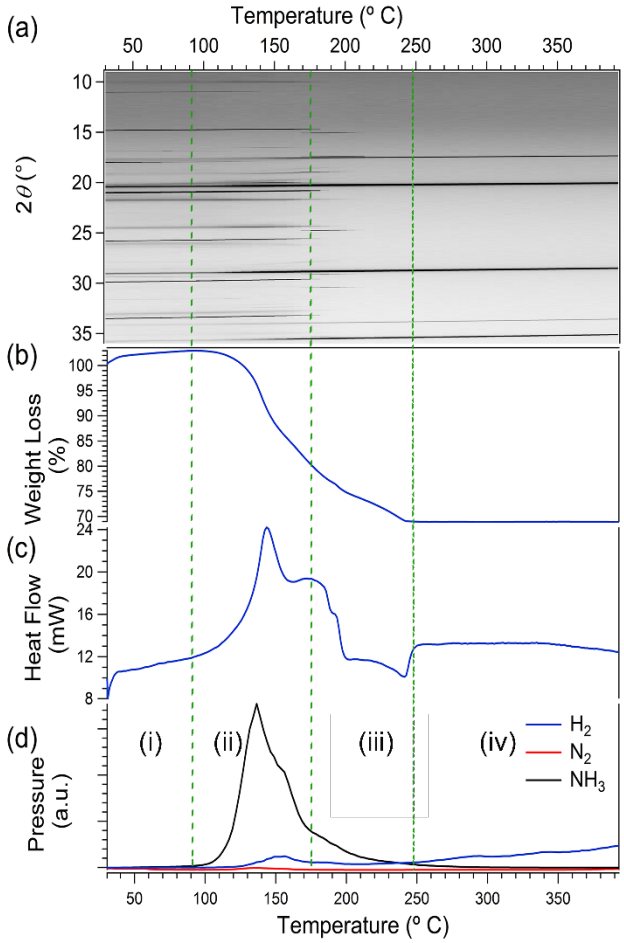

Fig. 4. (a) *In situ* SR-XRD data, (b) TGA, (c) DSC and (d) RGA data for NH_4Cl + $NaNH_2$. Region (i and ii): contains $NaNH_2$, LT-NH_4Cl, NaOH, an unknown and NaCl phases. Region (iii) contains NaCl and HT-NH_4Cl phases. Region (iv) contains NaCl. For complete phase identification of XRD data see Fig. S6†. $\Delta T/t$ = 5 °C/min. λ = 1.0003896(1) Å. Endothermic heat flow in the down direction for DSC data.

Thermal decomposition of $NH_4Cl + NaNH_2$

The SR-XRD pattern of the initial BM mixture of NH_4Cl and $NaNH_2$ indicates that some decomposition has occurred during milling with the observation of NaCl along with the NH_4Cl and $NaNH_2$ starting materials (Figs. 4a and S6†). In addition, impurity NaOH and another unknown phase were identified. Upon reaching ~146 °C during *in situ* SR-XRD measurements, all remnants of $NaNH_2$ had disappeared. At this point, excluding the unknown phase, the composition of the material determined by quantitative phase analysis is ~42.7(5) wt% of NH_4Cl, 28.7(4) wt% NaCl and 28.5(8) wt% NaOH. The LT to HT phase change for NH_4Cl begins at ~164 °C, while the HT-phase undergoes decomposition and is unidentifiable by ~215 °C. The NaOH and the unknown phase are no longer detected by ~190 and ~200 °C, respectively, leaving NaCl as the only crystalline phase. While it was not possible to index the Bragg peaks for the unknown phase, it is believed that it is a $Na(OH)_{1-x}(NH_2)_x$ phase.[44] The formation of this material during BM would also ascertain why NaCl is observed in the initial material.

Thermal decomposition of $NH_4Cl + LiNH_2$

The SR-XRD pattern of the ball milled mixture of NH_4Cl and$LiNH_2$ contains 57.4(1) wt% NH_4Cl, 20.3(1) wt% $LiNH_2$, 21.8(1) wt% LiCl, and 0.43(9) wt% Li_2O indicating that some decomposition occurred during the milling process (Figs. 5a and S7†). This assumption is corroborated by TGA data, in which a 38 wt% loss is observed rather than the theoretical value of 44.5 wt% (Fig. 5b). As the BM initial sample contained 21.8(1) wt% LiCl, assuming a 1:1 reaction product of LiCl:NH_3 (Table 1), this equates to 8.8 wt% NH_3 desorbed during milling, which is close to the difference between the measured and theoretical TGA capacities.

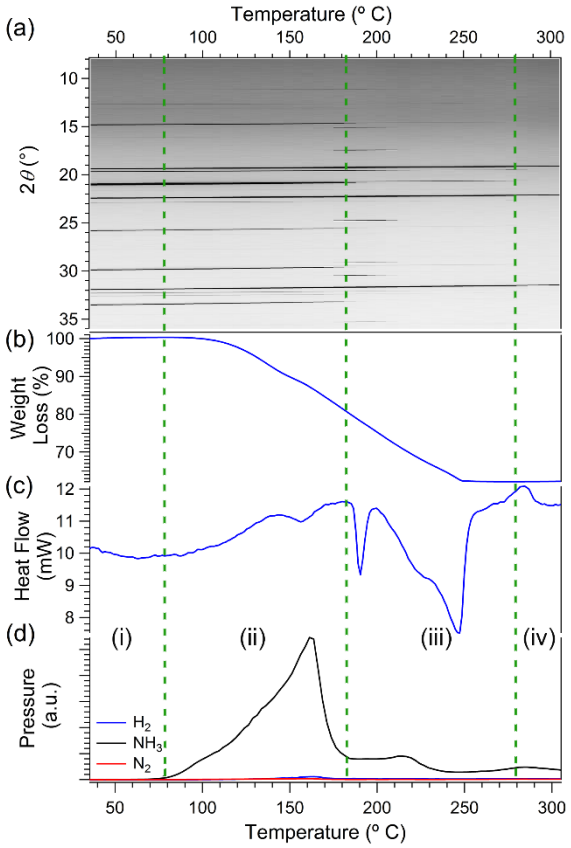

Fig. 5. (a) *In situ* SR-XRD data, (b) TGA, (c) DSC and (d) RGA data for $NH_4Cl + LiNH_2$. Region (i and ii): contains $LiNH_2$, LT-NH_4Cl, Li_2O, unknown and LiCl phases. Region (iii) contains $LiNH_2$, LiCl, Li_2O, unknown and HT-NH_4Cl phases. Region (iv) contains LiCl. For complete phase identification of XRD data see Fig. S7†. $\Delta T/t$ = 5 °C/min. λ = 1.0003896(1) Å. Endothermic heat flow in the down direction for DSC data.

Thermal analysis of the material by TGA indicates that the onset temperature of decomposition occurs at 80 °C (Fig. 5b). The broad exothermic event in the DSC data originating at 90 °C, with a maxima of 143 °C, is attributed to a slow reaction between NH_4Cl and $LiNH_2$, producing NH_3 gas (Fig. 5c). This step produces 9 wt% NH_3 between 80 and 152 °C. NH_3, along with a miniscule quantity of H_2, continues to be desorbed until 175 °C (Fig. 5d), at which point *in situ* XRD indicates that the phase change from LT-NH_4Cl to HT-NH_4Cl occurs with subsequent decomposition between ~180 and 210 °C (Figs. 5a and S7†). An endothermic peak is also observed in this regime, with a peak heat flow at 190 °C. The decomposition of $LiNH_2$ appears to be present until ~280 °C as observed in the *in situ* SR-XRD experiment, even after the decomposition of NH_4Cl at ~220 °C. In addition, three Bragg peaks of a minor unknown phase are observed at 14.6, 19.5, 20.8, 22.7 and 29.5° 2Θ. This phase increases in crystallinity from ~60 °C until disappearing at ~280 °C. The decomposition of NH_4Cl, $LiNH_2$ and the unknown phase explain the broad endothermic peak in the DSC data between 200 and 280 °C along with a concomitant slow release of NH_3. The decomposition temperature of lithium amide is therefore greatly reduced compared to that of the pure material, an effect that was also noted when exploring the effect of Cl^- on $LiNH_2$ with the addition of LiCl.[45]

Thermal decomposition of $2NH_4Cl + MgH_2$

The initial composition of the BM material measured by SR-XRD indicates that NH_4Cl, MgH_2 and Mg are present in the powder (Figs. 6a and S8†). *In situ* SR-XRD of the powder shows that the phase transition onset of LT-NH_4Cl to HT-NH_4Cl begins at ~176 °C with no more LT-NH_4Cl being observed at 197 °C. Any remnants of HT-NH_4Cl disappears at 248 °C. In addition to the NH_4Cl phase change and decomposition, a new phase emerges at 170 °C, which has a maximum intensity at ~242 °C and a decomposition temperature of 258 °C. This phase can be indexed to a tetragonal phase with lattice parameters of 5.01746(2), 5.01746(2), 16.2398(1) Å at ~240 °C corresponding to a possible space group of *I*4/*mmm*. A possible structure is $(NH_4)_2MgCl_4$ which is isomorphous with K_2MgCl_4.[46] MgH_2 appears to start decomposing at 190 °C and is last observed at 294 °C. During the decomposition regime of MgH_2 and the $(NH_4)_2MgCl_4$ phase, two unknown phases begins to appear at ~248 °C and disappear by 311 and 330 °C. Due to the analogous nature of $(NH_4)_2MgCl_4$ to the K_2MgCl_4 system, the unit cells for $K_3Mg_2Cl_7$ and $KMgCl_3$ were evaluated but not match either of the unknown phases.[47] In addition, $Mg(NH_3)_xCl_2$ (X = 1,2,4,6) were considered as potential side products in the reaction. Within this temperature range $Mg(NH_3)_2Cl_2$ is the only likely

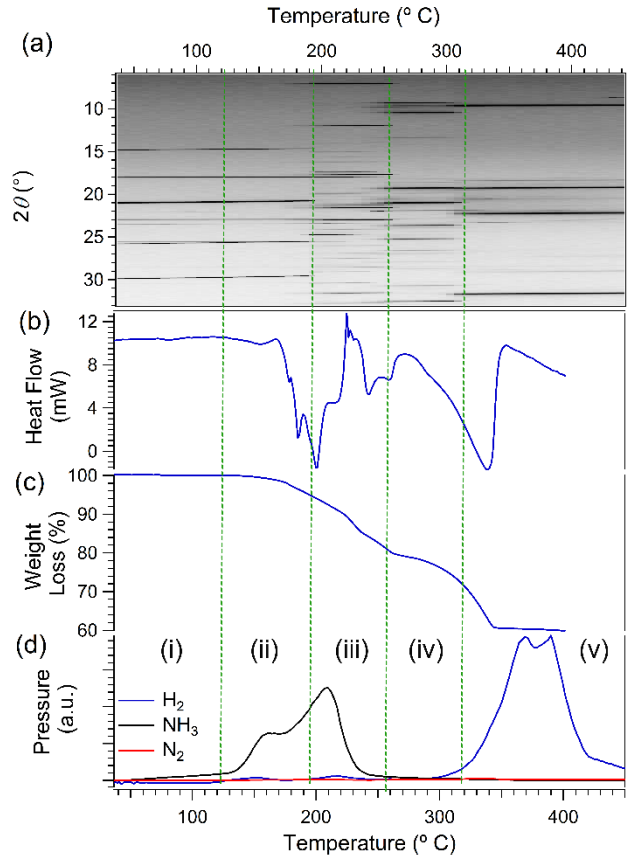

Fig. 6. (a) *In situ* SR-XRD data, (b) DSC, (c) TGA and (d) RGA data for $2NH_4Cl + MgH_2$. Region (i): contains MgH_2, Mg and LT-NH_4Cl phases. Region (ii): contains MgH_2, Mg, $(NH_4)_2MgCl_4$ and LT-NH_4Cl phases. Region (iii) contains MgH_2, $(NH_4)_2MgCl_4$, Mg and HT-NH_4Cl phases. Region (iv) contains MgH_2, Mg and two unknown phases. Region (v) contains $MgCl_2$, an unknown and Mg. For complete phase identification of XRD data see Fig. S8†. $\Delta T/t$ = 5 °C/min. λ = 1.0003896(1) Å. Endothermic heat flow in the down direction for DSC data.

compound to exist[48] and unfortunately none of the unknown phases match the measured lattice parameters or unit cell.[49] $MgCl_2$ is not observed until ~300 °C and is the major crystalline phase after 330°C, along with another minor unknown phase.

The thermal analysis data correlates extremely well with the crystallographic data, which shows that there are three distinct decomposition events, each containing multiple components (Fig. 6(b-d). The first event releases NH_3 and H_2 between ~125 to ~250 °C, as determined by RGA. DSC analysis identifies four endothermic maxima (177, 185, 200 and 215 °C), while TGA indicates a corresponding mass loss of 10.5 wt%. Between 225 and 238 °C, a mass loss of 4.5 wt% is observed, along with a triplet of exothermic peaks at 225, 228 and 232 °C. Between 238and 264 °C a doublet of endothermic events 243 and 259 °C and an associated mass loss of 5.2 wt% is observed. After 264 °C a large exothermic peak is determined with a maximum heat flow at 334 °C. The event continues until 355 °C where 10.8 wt% of NH_3 and H_2 is released. Overall, 40.4 wt% loss is detected by TGA despite a theoretical loss of 28.6 wt%. This would indicate a loss of a quarter of the Cl content, although analysis of the RGA for HCl and N_2 indicated no loss of gaseous Cl containing products. As construed in the reaction between NH_4Cl + LiH, it is possible that HCl may be produced during the decomposition of NH_4Cl causing a continued detection of H_2 throughout the remaining experiment.

Thermal decomposition of $2NH_4Cl + CaH_2$

Compared to the $2NH_4Cl + MgH_2$ mixture, the decomposition of $2NH_4Cl + CaH_2$ is relatively simple. The initial mixture was determined to contain only NH_4Cl (71.8(1) wt%) and CaH_2 (28.2(1) wt%), as expected, by SR-XRD (Figs. 7a and S9†). NH_3 and H_2 are observed by RGA starting at ~120 °C and both having maxima at 230 °C (Fig. 7b). A second NH_3 peak is observed at 273 °C and is no longer detected after 365 °C. H_2 meanwhile, is continuously evolved throughout experiment. The first indication of decomposition by TGA occurs at 152 °C, in which a mass loss of 30.1 wt% is achieved before 284 °C (Fig. 7b). The second mass loss step releases 8.6 wt% before 335 °C giving a total of 38.7 wt% mass loss. As observed with $2NH_4Cl + MgH_2$, the measured mass loss is greater than the theoretical value of 25.5 wt% and may be attributed to the loss of a quarter of the Cl content. Again, the RGA data indicated no evolution of HCl or N_2 although H_2 is observed throughout the experiment even after mass loss from the sample is complete.

During the DSC measurement, three endothermic events are observed with peak heat flows at 195, 280 and 329 °C (Fig. 7b). The peak at 195 °C corresponds to the decomposition of LT-

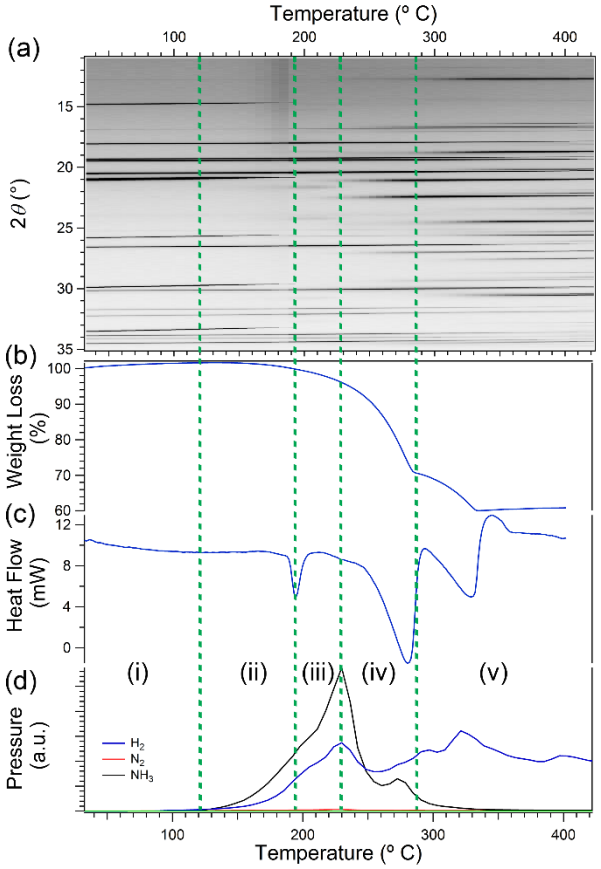

Fig. 7. (a) *In situ* SR-XRD data and (b) DSC-TGA-RGA data for $2NH_4Cl + CaH_2$. Region (i and ii): contains CaH_2 and LT-NH_4Cl phases. Region (ii): contains CaH_2, LT-NH_4Cl and NH_4CaCl_3 phases. Region (iii) contains CaH_2, HT-NH_4Cl and NH_4CaCl_3 phases. Region (iv) contains CaH_2, and two unknown phases. Region (v) contains CaH_2, CaHCl and $CaCl_2$. For complete phase identification of XRD data see Fig. S9†. $\Delta T/t$ = 5 °C/min. λ = 1.0003896(1) Å.

NH_4Cl, which is no longer observable by XRD after 203 °C. On this occasion, no phase change is observed from LT-NH_4Cl to HT-NH_4Cl by *in situ* SR-XRD. NH_4CaCl_3 (space group $Pm\bar{3}m$, isomorphous to $KCaCl_3$)[50] is observed from ~170 °C. This phase has a maximum intensity at ~207 °C and disappears by 227 °C. CaH_2 is observed from RT to 400 °C although the corresponding Bragg peaks begin to diminish at ~239 °C. CaH_2 is most likely to be the largest contribution to the second endotherm at 280 °C (see Fig. 7b). This temperature is considerably lower than that observed for pure CaH_2,[51] likely caused by the destabilising effect of the added NH_4Cl. The onset of decomposition for CaH_2 coincides with the onset of formation of CaHCl (space group $P4/nmm$)[52] and an unknown phase which are thermally stable up to at least 500 °C. $CaCl_2$ is observed to commence formation at 286 °C along with another unknown phase. One exothermic event is observed at 345 °C although the cause is unclear, it is most likely attributed to a phase change. The identity of the unknown phases were considered and attempts to index the peaks were made. Materials that were considered also include $CaCl_2{\cdot}(NH_3)_x$ (X = 2, 8).

Addition of Pd catalyst to NH_4Cl + NaH

In attempt to alter the reaction kinetics between the NH_4Cl and NaH and to cause preferential formation of H_2 and N_2 over NH_3, palladium (II) chloride was added (1 mol% and 10 mol%) as a potential catalyst to the NH_4Cl + NaH powder (Figs. 8, S10 and S11†). From *in situ* SR-XRD data, the NH_4Cl, NaH and 1 mol% $PdCl_2$ material does not show any observable Bragg peaks for $PdCl_2$ as it is below the limit of detection (Figs. 8a and S10†). LT-NH_4Cl phase transitions to the HT phase at ~176 °C, which also decomposes before ~206 °C. NaH is no longer visible in the XRD pattern by 214 °C. On the contrary, analysis of the BM mixture of NH_4Cl, NaH and 10 mol% $PdCl_2$ shows that minimal reaction has occurred between the starting reagents and only 3 wt% NaCl is present. As the sample is heated *in situ*, the intensity of $PdCl_2$ starts to decrease at ~130 °C and has disappeared by 155 °C (Figs. 8e and S11†). At the same time, Pd metal is observed and increases in intensity. The observed intensity of NaH begins to decrease from ~95 °C while it is no longer detected at the temperature of the LT-NH_4Cl to HT phase change at 176 °C. Once the HT-NH_4Cl has decomposed, ~227 °C, no further reaction occurs. Overall, the increment of 1 mol% $PdCl_2$ to 10 mol% does not alter the reaction pathway, but the temperatures at which reactions occur.

A comparison of the thermal analysis data (DSC-TGA and RGA) shows a stark contrast between the catalysed and uncatalysed NH_4Cl + NaH samples. The pure sample shows a peak gas desorption at ~170 °C while 1 mol% and 10 mol% have a

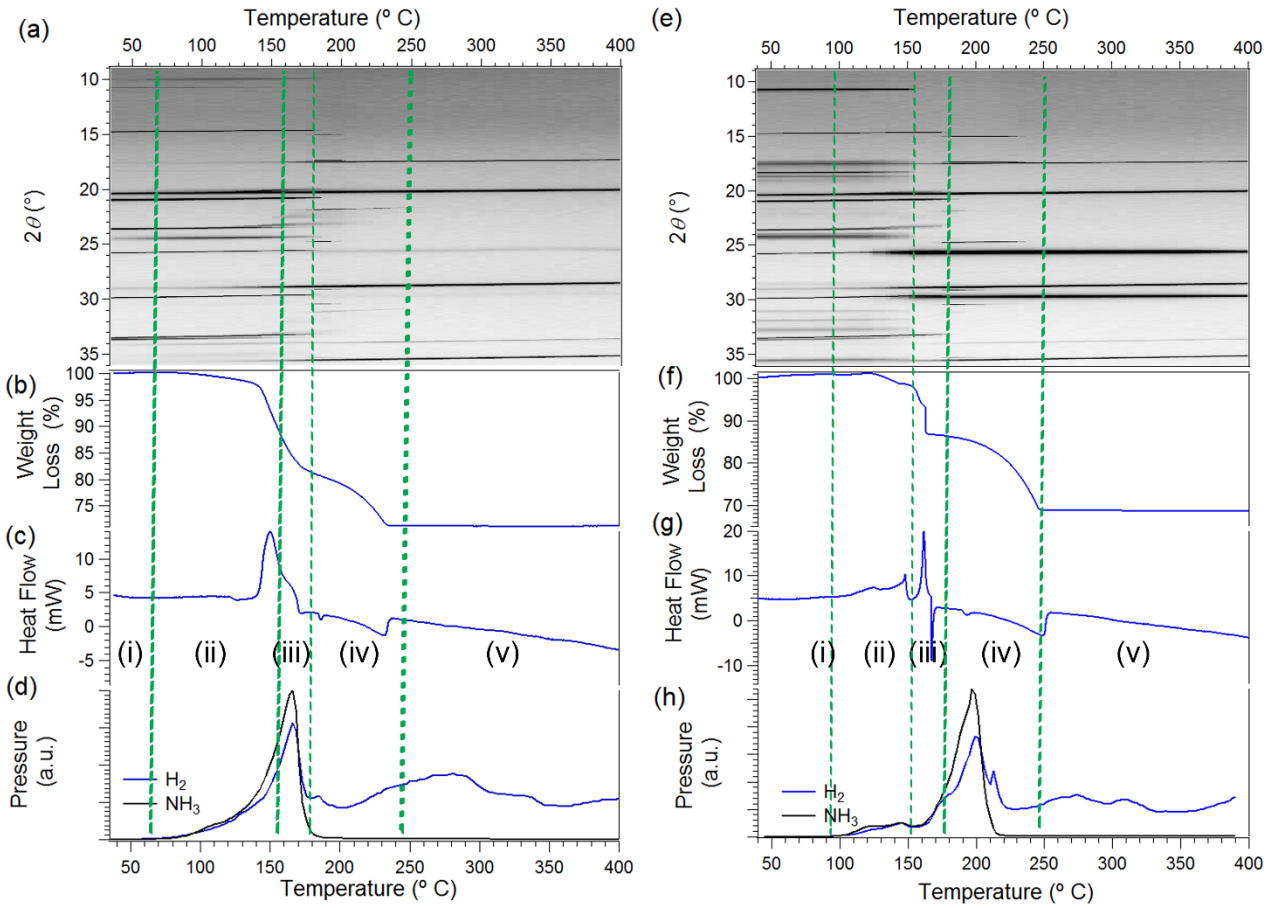

Fig. 8. (a – d) *In situ* SR-XRD data and DSC-TGA-RGA data for NH_4Cl + NaH + 1 mol% $PdCl_2$ and (e – h) NH_4Cl + NaH + 10 mol% $PdCl_2$. Region (i and ii): contains NaH, LT-NH_4Cl, $PdCl_2$ and NaCl phases. Region (iii) contains NaH, LT-NH_4Cl, Pd and NaCl phases. Region (iv) contains HT-NH_4Cl, Pd and NaCl phases (also NaH for 1 mol% $PdCl_2$ containing material). Region (v) contains NaCl. For complete phase identification of XRD data see Figs. S10 and S11†. $\Delta T/t$ = 5 °C/min for SR-XRD. λ = 1.0003896(1) Å. Endothermic heat flow in the down direction for DSC data

Journal Name

ARTICLE

maximum H_2 release at 166 and 198 °C, respectively. Inaddition, for the catalysed samples, H_2 continues to be detected until the end of the experiment. This is surprising as no crystallographic events at these temperatures during *in situ* SR-XRD. In addition, the measured mass loss for the 1mol % and 10 mol% catalysed systems is much greater than the theoretical mass loss. The 1 mol % $PdCl_2$ system loses 28.8 wt% while the theoretical mass loss is 24.3, whereas 31.2 wt% is measured compared to a theoretical quantity of 20.0 wt% for the 10 mol% system. As mentioned previously for the NH_4Cl mixed with MgH_2 or CaH_2, the elevated practical mass loss may be attributed to HCl loss. This gaseous acid reacts with the stainless-steel tubing producing hydrogen. It is noted that elevated mass loss occurs with increased addition of $PdCl_2$, with no difference in mass loss being observed when catalyst is not added to NH_4Cl + NaH. This is attributed to the NaH reacting with $PdCl_2$ rather than the intended NH_4Cl. The remaining NH_4Cl then decomposes as observed for the pure material (Fig. 1) producing HCl, although NH_3 is not observed during this process. Overall, this suggests that the addition of $PdCl_2$ does not incur splitting of NH_3 during desorption as discussed previously in the literature.[35]

The DSC data exhibits the largest contrast between samples. The pure and 1 mol% samples have a large exothermic peak between ~125 and 175 °C (Figs. 2c and 8c), whereas the 10 mol % sample exhibits two exothermic peaks in the same region with an additional sharp endothermic peak at ~165 °C (Fig. 8g). The mass loss for all three samples is completed between 225 and 250 °C.

Technological feasibility assessment

For energy storage materials to be utilised in technological applications, they must have a high energy density, be inexpensive, and usable within a practical temperature range. The materials employed in this study hold great potential for technological applications as they meet these demands. The US DOE has provided targets that hydrogen storage materials must meet to be used for vehicular applications, one of which is that the gas should be released between 40 and 85 °C.[53] The mixture of NH_4Cl + NaH has a decomposition onset temperature of ~90 °C, although peak gas evolution is not achieved until ~170 °C. Addition of 1 mol% $PdCl_2$ to NH_4Cl-NaH has a similar, albeit increased, onset decomposition temperature of ~65 °C although this incurs an increase in monetary price. The other *M*H's and *M*NH_2's investigated in this study have increased decomposition onset temperatures, compared to NH_4Cl-NaH, of between 72 and 125 °C, which is potentially useful. $2NH_4Cl$ + MgH_2 has the highest onset operating temperature of above 125 °C, making it the least likely to find application.

The cost of a fuel is a very important consideration when examining its viability compared to current fuel options. The US DOE has set an energy target cost of US$10/kWh. The energy target cost of these materials compare favourably to the US DOE target. NH_4Cl-NaH for instance, would cost US$1.25/kg of raw material.[38, 54] A 50:50 NH_3:H_2 combustion ratio would produce 14.7 MJ/kg (4.1 kWh/kg) of gas produced giving an overall cost of US$0.6/kWh (Table 1).[38] The cost of the other mixtures would be of similar size although sourcing industrial prices for these materials is troublesome. These prices would diminish further for large scale production of the materials. The $2NH_4Cl$-*M*H_2 (*M* = Mg, Ca) materials show excellent gravimetric capacity (40.4 and 41.4 wt%, respectively) and practical volumetric gas densities (607 and 657 kg/m^3, respectively). The cost of these *M*H's is also low with $2NH_4Cl$-CaH_2 and $2NH_4Cl$-MgH_2 costing US$0.5/kWh and US$0.3/kWh, respectively. LiH, $LiNH_2$ and $NaNH_2$ may have agreeable energy densities and decomposition temperatures but the price of the raw materials excludes them from contention. In addition, the long term utilisation of a lithium based material as a fuel source is not sustainable.[55]

A weakness of these materials is that they decompose over multiple steps. This may have a detrimental effect on the energy storage capacity because if the fuel is operated at lower temperatures, the onset of decomposition for the next step will not be reached resulting in a major reduction in efficiency.

The decomposition pathway and thermodynamics of these materials have been determined using HSC Chemistry software (Table S1†). Unfortunately, the database for this software did not contain many of the by-products experimentally observed including e.g. the Mg and Ca amides/imides, $(NH_4)_2MgCl_4$ and NH_4CaCl_3. The thermodynamic properties of many of these compounds are generally unknown and as a result accurate thermodynamic predictions could not be obtained. Theoretically the reactions are all exothermic with NH_4Cl + NaH having the largest predicted reaction enthalpy of −86.1 kJ/mol NH_4Cl. Experimentally many of the systems exhibit endothermic reactions although a precise determination of the thermodynamics could not be achieved due to the multiple steps of reaction and impurities within the samples. Comparing the Ca and Mg systems, it is clear that the experimental pathway is predominantly endothermic rather than exothermic. This is due to the mismatch between the theoretical and experimental reaction pathway.

Since the NH_4Cl-*M*H and NH_4Cl-*M*NH_2 materials form NH_3/H_2 gas mixtures during decomposition, the fuel produced could be burnt in an internal combustion engine to avoid poisoning of fuel cell membranes. Generally NH_3 has a narrow flammability limit of 15.5% to 27% volume in air,[20] which leads to a low

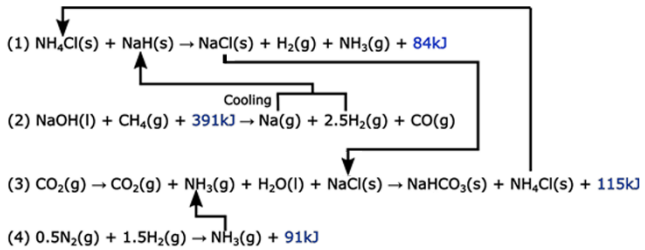

Fig. 9. Proposed reaction cycle for sodium chloride and ammonium chloride starting materials.

combustion rate. However, recent studies have shown that the presence of hydrogen during ammonia combustion can lower combustion temperatures and increase the burning velocity of ammonia flames.[56] These mixtures are theoretically producing a 50 mol% ratio of H_2 and NH_3 apart from $LiNH_2$ and $NaNH_2$ which are producing nearly 100 % NH_3. Therefore, these mixtures will allow efficient conversion of the gas fuel to energy to propel a vehicle without the formation of large quantities of NO_x or other products usually associated with combustion engines using petrol or diesel.

Upon refuelling the vehicle, the waste product removed would be the solid metal salt, e.g. NaCl, which is non-hazardous. Off-board regeneration of the waste product can also be considered to recycle this material using methods that are already used in large scale commercial processes. An example of a viable fuel cycle utilising commercial processes is exhibited in Fig. 9 with the reactions incorporated into the scheme outlined below. Ideally the hydrogen would be produced using renewable energy sources.

1) NH_3, H_2 and NaCl are produced from the reaction between NH_4Cl and NaH. NH_3 and H_2 are used for on-board fuel applications while NaCl is reprocessed.
2) Production of NaH from NaOH and CH_4 using the Power Ball process.[57] $NaOH_{(l)}$ is first reacted with $CH_{4(g)}$ to form $Na_{(g)}H_{2(g)}$ and $CO_{(g)}$. The $Na_{(g)}$ and $H_{2(g)}$ are then cooled and combined to form $NaH_{(s)}$. This method has the potential to reduce production costs compared to synthesis by common electrolysis. The left over $CO_{(g)}$ and $H_{2(g)}$ could then be used to produce $CO_{2(g)}$ and more $H_{2(g)}$ via the Water Shift reaction.[58]
3) Regeneration of NH_4Cl from NaCl via the Solvay process using NH_3, CO_2 and H_2O.[59]
4) NH_3 generated from N_2 and H_2 using the Haber-Bosch process[22] or electrochemical synthesis.[60]

Conclusions

This study has explored the reactions of four ammonium chloride – metal hydride (NH_4Cl-*M*H) and two ammonium chloride – metal amide (NH_4Cl-*M*NH_2) powders for potential use as solid-state ammonia and hydrogen fuel sources for vehicular applications. Comparison of the results to US DOE guidelines for vehicles running on gas reveals that these materials exceed targets with respect to cost of materials, fuel capacity and operating temperature. DSC-TGA and RGA analysis indicates that the onset of H_2 and/or NH_3 release occurs at ~90 °C for NH_4Cl-NaH with an average of 97 °C for all materials in the study. TGA analysis revealed a high gravimetric gas evolution ranging between 24.8 wt% for NH_4Cl-NaH and 41.4 wt% for $2NH_4Cl$-CaH_2 providing exceptional volumetric gas densities of 363 and 657 kg/m^3, respectively. This far exceeds densities of pure NH_3, H_2 or metal hydride materials such as Mg_2FeH_6.

In situ synchrotron powder X-ray diffraction of each of the materials shows that the metal hydrides decompose at significantly lower temperatures compared to their pure counterparts with the reaction with NH_4Cl enhancing the decomposition process. The final products after a full reaction are the metal hydride salts with no other by-products. This will allow for the products to be recycled in an off-board process.

Each of the NH_4Cl-*M*H or NH_4Cl-*M*NH_2 materials released NH_3 and H_2 upon reaction apart from $NaNH_2$ and $LiNH_2$. To determine if the NH_4Cl-NaH mixture could be catalytically prevented from forming NH_3, $PdCl_2$ was added. Unfortunately, this resulted in a slight increase in the onset temperature of desorption with NH_3 still being released. Further investigation into alternative catalysts such as Ru based compounds may alter the decomposition pathway. NH_4Cl alone could not be used in a system as the decomposition process involves the formation of HCl. No acid was identified in the decomposition process of the NH_4Cl-*M*H or NH_4Cl-*M*NH_2 systems.

The high gravimetric capacity of the materials along with the low cost of NH_4Cl allows for the overall cost to meet US DOE targets of US$10/kWh. NH_4Cl-NaH has a material cost of US$0.6/kWh while $2NH_4Cl$-CaH_2 and $2NH_4Cl$-MgH_2 cost US$0.5/kWh and US$0.3/kWh, respectively. A recycling process has been identified for the NH_4Cl-NaH material using industrial processes already developed. This will decrease the overall cost of the system, which is already estimated to meet targets set by the US DOE. If the industrial process is to be scaled up further, the cost of these metal hydrides should decrease causing this fuel to be even more competitive in the future. Overall, the reaction cycle potentially allows carbon-neutral regeneration of the starting materials, making it a sustainable energy option.

Conflicts of interest

There are no conflicts to declare.

Acknowledgements

CEB, TDH, DAS and VS acknowledge the financial support of the Australian Research Council (ARC) for ARC Linkage grant LP120101848, LP150100730 and ARC LIEF grant LE0989180. HS acknowledges the Department of Physics and Astronomy at Curtin University for providing support through the Summer Physics and Astronomy Scholarship. DAS acknowledges the financial support of a Curtin University Postdoctoral Research Fellowship. The authors also acknowledge funding from the Australian Synchrotron (ANSTO), which enabled the research at the powder diffraction beamline to be undertaken.

Notes and references

1 H. Khatib, *Energy policy*, 2012, **48**, 737-743.
2 L. Schlapbach and A. Zuttel, *Nature*, 2001, **414**, 353-358.
3 D. A. Sheppard, M. Paskevicius, T. D. Humphries, M. Felderhoff, G. Capurso, J. Bellosta von Colbe, M. Dornheim, T. Klassen, P. A. Ward, J. A. Teprovich, C. Corgnale, R. Zidan, D. M. Grant and C. E. Buckley, *Appl. Phys. A*, 2016, **122**, 395.
4 K. T. Møller, T. R. Jensen, E. Akiba and H.-w. Li, *Prog. Nat. Sci.*, 2017, **27**, 34-40.
5 A. Zuttel, A. Remhof, A. Borgschulte and O. Friedrichs, *Phil. Trans. R. Soc. A*, 2010, **368**, 3329-3342.
6 G. W. Crabtree, M. S. Dresselhaus and M. V. Buchanan, *Physics Today*, 2004, **57**, 39-44.
7 B. R. S. Hansen, M. Paskevicius, H.-W. Li, E. Akiba and T. R. Jensen, *Coord. Chem. Rev.*, 2016, **323**, 60-70.
8 T. D. Humphries, D. A. Sheppard and C. E. Buckley, *Coord. Chem. Rev.*, 2017, **342**, 19-33.
9 S. Orimo, Y. Nakamori, J. R. Eliseo, A. Zuttel and C. M. Jensen, *Chem. Rev.*, 2007, **107**, 4111-4132.
10 C. Frommen, M. H. Sørby, M. Heere, T. D. Humphries, J. E. Olsen and B. C. Hauback, *Energies*, 2017, **10**, 2115.
11 T. D. Humphries, D. A. Sheppard, G. Li, M. R. Rowles, M. Paskevicius, M. Matsuo, K.-F. Aguey-Zinsou, M.-V. Sofianos, S.-i. Orimo and C. E. Buckley, *J. Mater. Chem. A*, 2018, **6**, 9099-9108.
12 M. Fellet, C. E. Buckley, M. Paskevicius and D. A. Sheppard, *MRS Bulletin*, 2013, **38**, 1012-1013.
13 D. A. Sheppard, T. D. Humphries and C. E. Buckley, *Appl. Phys. A*, 2016, **122**, 406.
14 W. I. F. David, J. W. Makepeace, S. K. Callear, H. M. A. Hunter, J. D. Taylor, T. J. Wood and M. O. Jones, *J. Am. Chem. Soc.*, 2014, **136**, 13082-13085.
15 A. Klerke, C. H. Christensen, J. K. Norskov and T. Vegge, *J. Mater. Chem.*, 2008, **18**, 2304-2310.
16 T. Zhang, H. Miyaoka, H. Miyaoka, T. Ichikawa and Y. Kojima, *ACS Applied Energy Materials*, 2018, **1**, 232-242.
17 Outukumpu, HSC Chemistry, 6.1, 2006.
18 L. Green, *Int. J. Hydrogen Energy*, 1982, **7**, 355-359.
19 J. Lee, S. Lee and O. Kwon, *Int. J. Hydrogen Energy*, 2010, **35**, 11332-11341.
20 J. Li, H. Huang, N. Kobayashi, Z. He, Y. Osaka and T. Zeng, *Energy*, 2015, **93**, 2053-2068.
21 A. Afif, N. Radenahmad, Q. Cheok, S. Shams, J. H. Kim and A. K. Azad, *Renew. Sustainable Energy Rev.*, 2016, **60**, 822-835.
22 J. M. Modak, *Resonance*, 2002, **7**, 69-77.
23 Indicative Chemical Prices A-Z. , http://www.icis.com/chemicals/channel-info-chemicals-a-z/. (accessed 12/02/2018).
24 E. Matthews, *Global Biogeochem. Cycles*, 1994, **8**, 411-439.
25 P. J. Feibelman, *Physics Today*, 2005, **58**, 13-14.
26 Praxair, Ammonia, anhydrous. Safety Data Sheet P- 4562, http://www.praxair.com/-/media/documents/sds/ammonia-nh3-safety-data-sheet-sds-p4562.pdf, (accessed 12/02/2018).
27 R. Lan, J. T. Irvine and S. Tao, *Int. J. Hydrogen Energy*, 2012, **37**, 1482-1494.
28 J. Yang, P. R. Beaumont, T. D. Humphries, C. M. Jensen and X. Li, *Energies*, 2015, **8**, 9107.
29 L. H. Jepsen, M. B. Ley, Y.-S. Lee, Y. W. Cho, M. Dornheim, J. O. Jensen, Y. Filinchuk, J. E. Jørgensen, F. Besenbacher and T. R. Jensen, *Mater. Today*, 2014, **17**, 129-135.
30 L. H. Jepsen, M. B. Ley, Y. Filinchuk, F. Besenbacher and T. R. Jensen, *ChemSusChem*, 2015, **8**, 1452-1463.
31 J. W. Makepeace, T. J. Wood, H. M. Hunter, M. O. Jones and W. I. David, *Chemical Science*, 2015, **6**, 3805-3815.
32 *US Pat.,* US7157166B2, 2007.
33 K. E. Lamb, D. M. Viano, M. J. Langley, S. S. Hla and M. D. Dolan, *Ind. Eng. Chem. Res.*, 2018, **57**, 7811-7816.
34 H. Miyaoka, H. Miyaoka, T. Ichikawa, T. Ichikawa and Y. Kojima, *Int. J. Hydrogen Energy*, 2018, **43**, 14486-14492.
35 L. Li and J. A. Hurley, *Int. J. Hydrogen Energy*, 2007, **32**, 6-10.
36 Z. Xueping, M. Qiuhua, F. Zhen, M. Feng, L. Shenglin, F. Xin, X. Guo and Z. Jiaojiao, *Rare Metal Materials and Engineering*, 2014, **43**, 2075-2078.
37 S. Mukherjee, S. V. Devaguptapu, A. Sviripa, C. R. F. Lund and G. Wu, *Applied Catalysis B: Environmental*, 2018, **226**, 162-181.
38 Price of chemicals, https://www.alibaba.com, (accessed 19/08/2018).
39 K. S. Wallwork, B. J. Kennedy and D. Wang, *Synchrotron Radiation Instrumentation: Ninth International Conference on Synchrotron Radiation Instrumentation*, 2007, **879**, 879-882.
40 P. D. Pathak and N. G. Vasavada, *Acta Crystallogr A*, 1970, **26**, 655-658.
41 I.-K. Suh, H. Ohta and Y. Waseda, *J. Mater. Sci.*, 1988, **23**, 757-760.
42 R. Farasat, B. Yancey and S. Vyazovkin, *J. Phys. Chem. C*, 2013, **117**, 13713-13721.
43 N. W. Luft, *Industrial Chemistry*, 1955, **31**, 502.
44 L. H. Jepsen, P. Wang, G. Wu, Z. Xiong, F. Besenbacher, P. Chen and T. R. Jensen, *Phys. Chem. Chem. Phys.*, 2016, **18**, 25257-25264.
45 J. Zhang and Y. H. Hu, *Ind. Eng. Chem. Res.*, 2011, **50**, 8058-8064.
46 C. S. Gibbons, V. C. Reinsborough and W. A. Whitla, *Can. J. Chem.*, 1975, **53**, 114-118.
47 G. S. Perry and H. Fletcher, *J. Phase Equilib.*, 1993, **14**, 172-178.
48 H. Zhu, X. Gu, K. Yao, L. Gao and J. Chen, *Ind. Eng. Chem. Res.*, 2009, **48**, 5317-5320.
49 A. Leineweber, M. W. Friedriszik and H. Jacobs, *J. Solid State Chem.*, 1999, **147**, 229-234.
50 H. J. Seifert, H. Fink, G. Thiel and J. Uebach, *Z. Anorg. Allg. Chem.*, 1985, **520**, 151-159.
51 R. W. Curtis and P. Chiotti, *J. Phys. Chem.*, 1963, **67**, 1061-1065.
52 P. Ehrlich, B. Alt and L. Gentsch, *Z. Anorg. Allg. Chem.*, 1956, **283**, 58-73.
53 DOE Technical Targets for Onboard Hydrogen Storage for Light-Duty Vehicles, https://www.energy.gov/eere/fuelcells/doe-technical-targets-onboard-hydrogen-storage-light-duty-vehicles, (accessed 12/03/2018).
54 J. P. DiPietro and E. G. Skolnik, 2000.
55 D. Abbott, *Proc. IEEE*, 2010, **98**, 42-66.
56 J. Li, H. Huang, N. Kobayashi, Z. He and Y. Nagai, *International Journal of Energy Research*, 2014, **38**, 1214-1223.
57 E. Skolnik, *Proceedings of the DOE*, 2000.
58 J. Xu and G. F. Froment, *AIChE J.*, 1989, **35**, 88-96.
59 G. Steinhauser, *Journal of Cleaner Production*, 2008, **16**, 833-841.
60 S. Giddey, S. P. S. Badwal, C. Munnings and M. Dolan, *ACS Sustainable Chemistry & Engineering*, 2017, **5**, 10231-10239.